

Toward $\Phi 56$ mm Al-Polar AlN Single Crystals Grown by the Homoepitaxial PVT Method

Danyang Fu, Dan Lei, Zhe Li, Gang Zhang, Jiali Huang, Xiaojuan Sun, Qikun Wang, Dabing Li, Jiang Wang,* and Liang Wu*



Cite This: *Cryst. Growth Des.* 2022, 22, 3462–3470



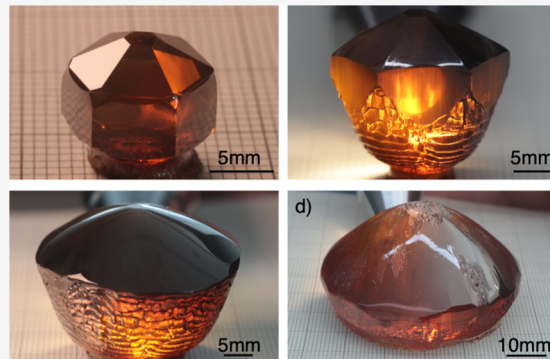
Read Online

ACCESS |

Metrics & More

Article Recommendations

ABSTRACT: Crack-free and parasitic-free Al-polar aluminum nitride (AlN) single crystals up to $\Phi 56$ mm were iteratively grown by the homoepitaxial physical vapor transport method. The detailed iterative growth processes from the spontaneous AlN boules to $\Phi 56$ mm single crystals were presented. Our growth experiments revealed that stable growth of large Al-polar crystals with good structural quality and UV transparency was possible using a pure tungsten setup. For each iteration, the initial expansion angle, which was dominated by the radial temperature gradient (ΔT_r), reached 50–60° under our specific growth system and growth conditions and then gradually decreased to 10–20° during the growth process. For all as-grown crystals, mirror-like facets with a step-flow growth mode could be observed. However, the {1010} side planes were strongly suppressed when using larger AlN seeds. Material characterization showed that the full width at half maximum of symmetric and asymmetric high-resolution X-ray diffraction rocking curves was 84–144 arcsec and 45–70 arcsec, respectively. The average etch pit density evaluated by preferential chemical etching was approximately $8.5 \times 10^4 \text{ cm}^{-2}$. The optical transmission spectra revealed that the entire wafer exhibited excellent ultraviolet (UV) transparency, with absorption coefficients of 19–29 cm^{-1} in the UV range of 4.43–4.77 eV (260–280 nm).



1. INTRODUCTION

Ultrawide band gap (UWBG) semiconductors have attracted extensive attention due to a broad range of potential applications in high-power, high-frequency, and high-voltage electronics and in deep ultraviolet (UV) optoelectronics.¹ As a promising UWBG semiconductor material, AlN offers compelling advantages over other semiconductor materials, such as a wide direct band gap (6.2 eV), high thermal conductivity (3.2 W/cm K), high electron drift velocity, high breakdown voltage, high chemical and thermal stability, excellent second-order optical nonlinearity, and prominent UV transparency.^{2–4}

In recent decades, various methods have been developed to prepare AlN crystals, such as hydride vapor phase epitaxy,^{5–7} flux/solution growth,^{8–10} and physical vapor transport (PVT) growth.^{11,12} Among these methods, the PVT method is considered to be the most promising technique for bulk AlN growth. Homoepitaxial growth using high-quality native seeds is the ultimate approach to grow high-quality large AlN crystals.^{13–15} The PVT method for bulk AlN crystal growth was developed by Slack and McNelly in 1976.¹¹ Since then, numerous efforts have been made to develop high-quality, large AlN crystals.^{2,12} Significant breakthroughs were made in

2008 by Bondokov et al.,¹³ Mueller et al.,¹⁴ and Schujman et al.,¹⁵ who successfully produced 2 in. AlN single-crystal wafers with a useable area of 85% through process optimization. Later, Dalmau et al.¹⁶ obtained a 47 mm high-quality single-crystal boule by homoepitaxial seeded growth in 2018, and Wang et al.¹⁷ obtained crack-free AlN single-crystalline wafers up to 60 mm in diameter with excellent deep-UV transparency and decent quality in 2019, although the exact growth process has not yet been provided.

AlN-based deep-UV light emitting diodes (DUV-LEDs) have attracted much attention and are expected to replace mercury-vapor lamps for sterilization, water purification, and biochemical sensors. However, the transparency issue of AlN substrates has been considered one of the key obstacles to fabricating high-external quantum efficiency DUV-LEDs.¹⁸ It is reported that the growth setup, growth process, and seed

Received: February 24, 2022

Revised: March 30, 2022

Published: April 11, 2022



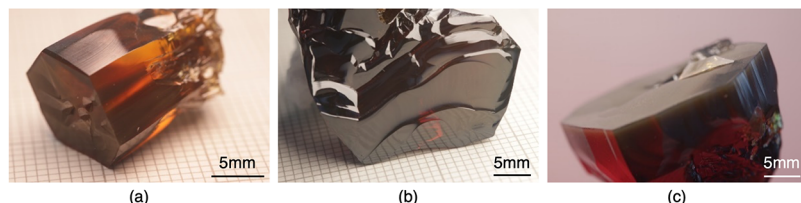


Figure 1. First-generation AlN boules with diameters of 12 (a), 23 (b), and 25 mm (c) prepared by the spontaneous PVT method (grid size of 1 mm).

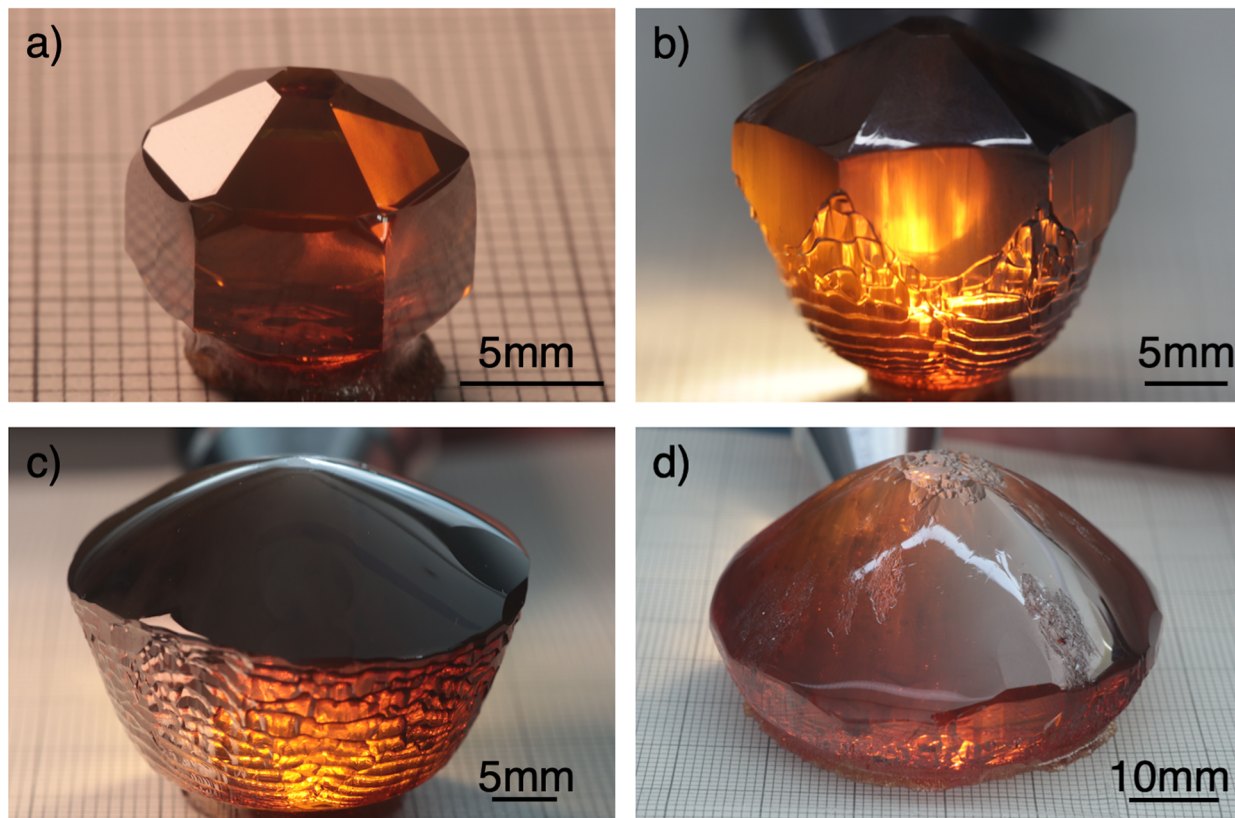


Figure 2. Various Al-polar AlN single crystals with diameters of 12 (a), 26 (b), 36 (c), and 56 mm (d) prepared by homoepitaxial PVT growth (grid size of 1 mm).

polarities have a significant effect on the UV transparency of AlN crystals. In particular, crystal polarity is a key factor in controlling the AlN surface morphology and growth mechanism, since it strongly impacts the incorporation of unintentionally doped impurities (O, C, and Si) in AlN crystals and their interplay with intrinsic point defects and, hence, the electrical and optical properties of AlN.^{18–20} Control of polarity is also essential for device design due to the strong polarization-induced internal electric fields.²¹ The experimental results of Filip et al.¹⁹ in a tungsten setup using Al-polar, N-polar, and mixed-polar seeds showed that the colorless or light brown Al-polar crystals have better light transmission than the dark brown N-polar crystals. In general, the growth of N-polar crystals is more likely to introduce carbon/oxygen impurities and point defects, which result in low UV transmission, although N-polar growth can usually maintain a stable and uniform step-flow growth mechanism.^{18,20,22,23} In contrast, Al-polar crystals prefer to grow by the three-dimensional (3D) island growth mode with multisite nucleation, which usually leads to a decrease in crystal size, quality, and growth uniformity.^{24,25}

In this paper, we report crack-free and parasitic-free Al-polar AlN single crystals up to $\Phi 56$ mm using an iterative homoepitaxial growth technique by the PVT method for the first time. The detailed iterative growth processes from the first-generation spontaneous AlN seeds to $\Phi 56$ mm boules were presented, and the growth habit and diameter enlargement behavior were investigated. Material characterization was also conducted to evaluate the obtained crystals.

2. EXPERIMENTAL PREPARATION

2.1. Growth Reactor Description. All growth experiments were conducted in resistive growth reactors at Ultratrend Technologies Inc. (model type UTI-PVT-D075H) capable of sustaining temperatures up to 2500 °C. The growth reactor consists of a tungsten crucible, two resistive heaters, and tungsten thermal insulators. Two pyrometers and one W–Re thermocouple were employed to measure temperatures at the crucible top and bottom and side tungsten heat shields, respectively. The entire growth system includes a growth atmosphere control system, a cooling system, a resistive heating system, and a motor system of the growth reactor, with each system being interconnectable and capable of automatically maintaining the required growth conditions. During the crystal growth process, the

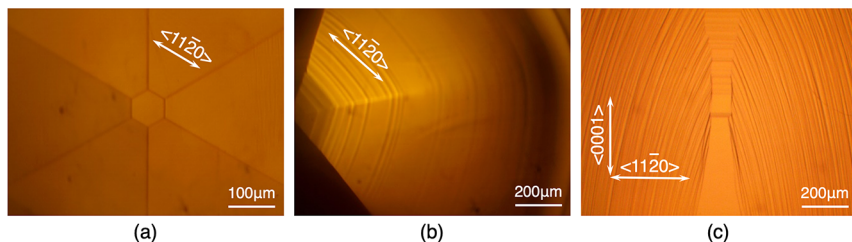


Figure 3. Optical micrographs of as-grown Al-polar AlN surface morphologies and growth steps.

crucible thermal field was adjusted by changing the position of the crucible relative to the heater using a motor system. More details of the growth reactor are described elsewhere.^{26–28}

2.2. Hot Zone and Crucible System Design and Optimization. One key issue of AlN homoepitaxy is parasitic growth, since the growth of parasitic grains along a random orientation is generally faster than *c*-plane growth. When the parasitic grains contact the growing single-crystalline AlN at any time during the growth process, normal *c*-plane growth will be disturbed. As a consequence, the crystal structural quality will decrease, and additional stress and defects and cracks will be generated. It has been reported that homoepitaxy on Al-polar surfaces typically exhibits 3D island growth accompanied by numerous growth centers.^{24,25} This growth mechanism normally occurs due to high supersaturation, which can lead to low crystal structural quality. It is common knowledge that low supersaturation at the growth surface can be achieved by reducing the axial temperature gradient (ΔT_a). However, ΔT_a is positively correlated with the axial growth rate (V_a), and a trade-off between ΔT_a and V_a is necessary. Due to the low supersaturation of the $\{10\bar{1}0\}$ surface perpendicular to the Al-polar growth plane, AlN crystals normally exhibit a low radial growth rate (V_r). A sufficiently high radial temperature gradient (ΔT_r) around the seed surface is necessary for reasonable crystal diameter expansion, although a large ΔT_r can lead to additional defects, such as low-angle grain boundaries (LAGBs) or basal plane dislocations (BPDs).^{29–31}

Considering the abovementioned, we designed a proprietary hot-zone setup and crucible system and optimized it using FEMAG software and a series of in-house finite element codes, including a mass transfer module,^{28,32} an impurity transport module,²⁷ an anisotropic 3D stress module,^{33–35} and a growth rate and supersaturation prediction module.³⁶ In particular, a seed holder that can sustain positive supersaturation only at the seed deposition surface was designed to prevent any parasitic nucleation adjacent to the growing AlN seed and therefore to completely eliminate parasitic polycrystalline growth on the periphery of AlN boules.³⁶ These efforts and details are not repeated for brevity.

2.3. AlN Powder Source and Seed Preparation. High-purity AlN powder (<20 ppm wt carbon, <100 ppm wt oxygen) was obtained by multiple sublimation recrystallization.²⁷ First-generation AlN boules with a maximum diameter of approximately 1 in. were prepared using our proprietary spontaneous growth technique,³⁷ as illustrated in Figure 1, and the (0002) full width at half maximum (fwhm) values of these spontaneous seeds evaluated by high-resolution X-ray diffraction (HRXRD) are smaller than 100 arcsec (not shown). *c*-plane seeds employed for subsequent homoepitaxial runs were fabricated from AlN boules grown either by spontaneous or homoepitaxial growth by following a common wafering process. Each seed, with the Al-polar surface upside down, was mounted on the aforementioned seed holder either by a mechanical, chemical, or thermal approach.

3. GROWTH RESULTS AND DISCUSSION

Except for the first-generation seed boules, all AlN crystals presented below (Figure 2) are as-grown by the homoepitaxial PVT method under a high-purity nitrogen atmosphere (99.999%) at 50–90 kPa. The growth temperature, which was determined through a combination of simulation

calculations and experimental data, varied between 2200 and 2300 °C. For all growth runs, the Al-polar facet was the deposition surface, and the average growth rate was evaluated to be 150–200 μm/h.

Figure 2 illustrates crack-free and parasitic-free AlN single crystals with diameters from Φ12 mm to Φ56 mm obtained iteratively by the homoepitaxial growth process. Figure 2a,b shows that the two as-grown crystals have a perfect hexagonal pyramid shape with a mirror-like flat top and are bounded with vertical prismatic $\{10\bar{1}0\}$ and rhombohedral $\{10\bar{1}L\}$ ($L = 1, 2, 3$) facets, hereafter referred to as *m*-plane and *r*-plane facets for simplicity, respectively. Similar results in a pure tungsten setup were demonstrated by Lu et al.³⁸ in 2009, but the crystal diameter was limited to approximately 12 mm. Large Al-polar AlN crystals (shown in Figure 2b) with perfect hexagonal shapes grown in a pure tungsten setup are rarely reported.

In general, N-polar growth is considered to be more suitable for crystal diameter enlargement with an extension angle of 10–30°,^{39–41} whereas Al-polar growth leads to a reduction in the crystal diameter. Our practical Al-polar growth experiments showed that the crystal diameter enlarged rapidly at the initial growth stage with an expansion angle larger than 50° for nearly all AlN boules. At this stage, the formation of prismatic *m*-facets was suppressed due to a convex local thermal field around the seed (not shown). However, the diameter expansion decreased significantly as soon as the *m*-facets formed when the radial thermal gradient (ΔT_r) was small, since the growth rate of the *m*-facets was an order of magnitude lower than that on the basal plane, particularly for smaller seeds. Nevertheless, the as-grown crystals failed to exhibit complete *m*-facets and *r*-facets for the homoepitaxial growth runs when larger seeds were used due to the increase in ΔT_r , as shown in Figure 2c,d. It should be noted that a noticeable rough surface was observed for the Φ56 mm AlN single crystal. We speculated that the rough surface was due to a stronger thermal transient effect for larger Al-polar crystal growth during the growth process, resulting in a weak facet growth stability incurred by nonuniform supersaturation and impurity evaporation.

The as-grown Al-polar crystal surface morphologies studied by optical microscopy showed that only one major growth center was observed on the top hexagonal mirror-like *c*-planes (as shown in Figure 3a), and pyramids were formed by macroscopic faceting of step bunching or growth steps (as illustrated in Figure 3b). Similar to *c*-plane N-polar growth, Al-polar growth was also initiated and spirally grew from a single growth center (or pre-existing threading screw dislocation), allowing a step-flow growth mechanism to avoid numerous growth centers and kinetic roughening.²³ We attributed this Al-polar step-flow growth mode to the sufficiently low supersaturation on the growth surfaces simulated by our in-house code (not shown). In contrast to that of the *c*-facet, the

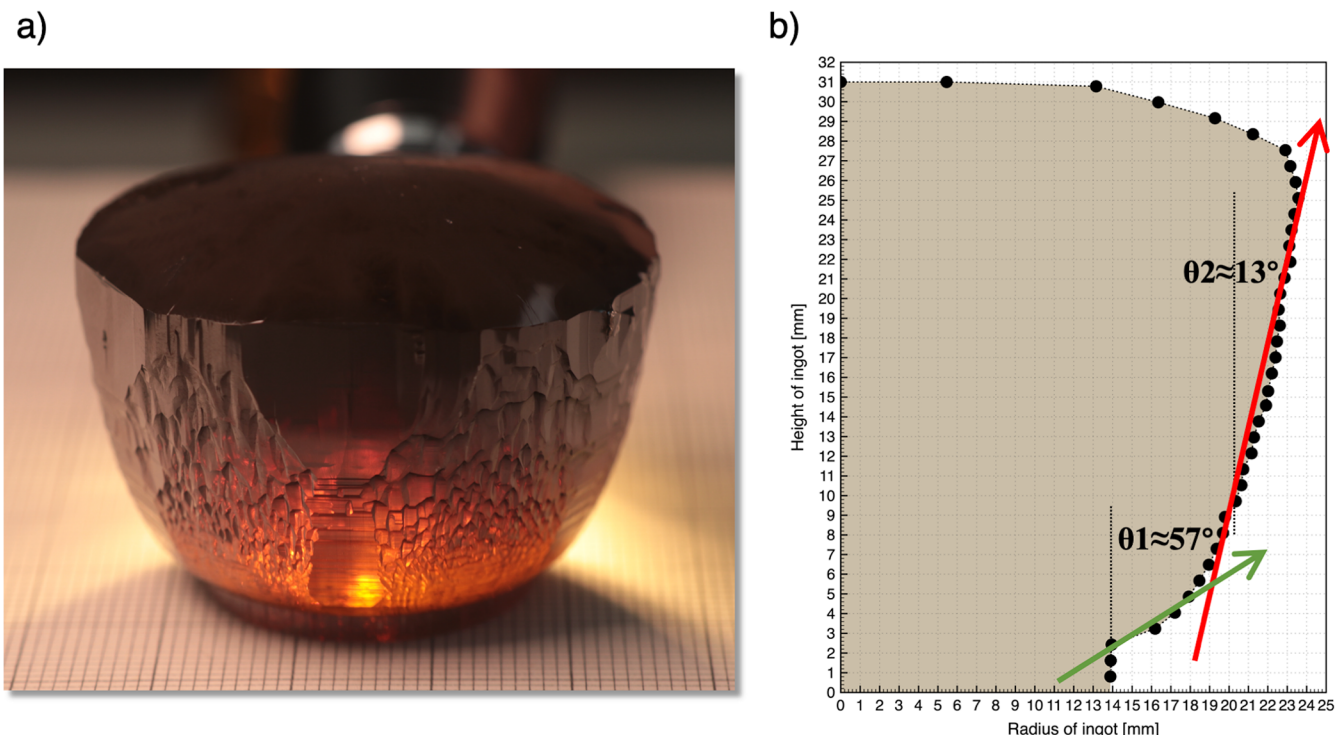


Figure 4. Size evolution of a 47 mm boule grown homoepitaxially on a 28 mm AlN seed.

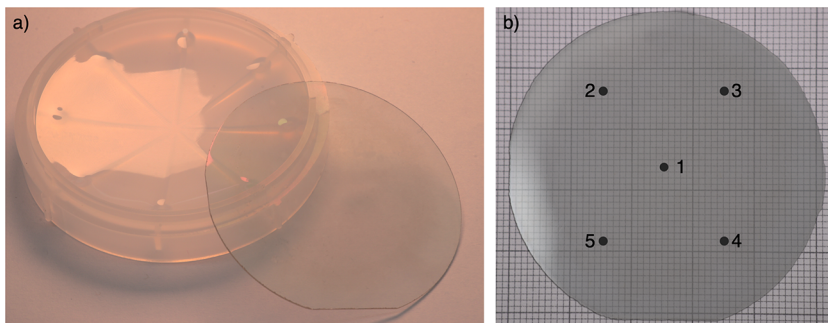


Figure 5. (a) Optical micrographs of an on-axis $0.6 \times 50.8 \text{ mm}^2$ AlN sample wafer cut from a $\Phi 56 \text{ mm}$ boule. (b) Size measurement of the wafer (grid size of 1 mm, $\approx 100\%$ useable area) and five labeled locations for characterization.

growth mode of the m -facets is two-dimensional (2D) step-flow, with each m -facet revealing a symmetrical growth center elongated in the c -direction (as illustrated in Figure 3c). Essentially similar growth conditions at the growth centers on the six prismatic facets resulted in the crystal habit exhibiting a perfect regular hexagon (as illustrated in Figure 2a,b). Furthermore, the widths of the growth steps in the c - and r -directions of the m -plane are different, which is mainly due to the different migration energies of atoms in each direction.

Figure 4 illustrates the detailed diameter evolution of a 47 mm Al-polar boule grown homoepitaxially on a 28 mm AlN seed. The initial expansion angle reached 57° and then gradually decreased to 13° during the growth process. ΔT_r plays a dominant role in the crystal growth habit. Compared with the boules in Figure 2a,b, the m -facets are suppressed due to a larger ΔT_r .

4. MATERIAL CHARACTERIZATION

All obtained AlN single-crystalline boules were sliced and then fabricated into wafers by following a standard wafering process

using our proprietary grinding and chemical mechanical polishing (CMP) techniques. One 2 in. AlN wafer with a thickness of $600 \mu\text{m}$ obtained from the $\Phi 56 \text{ mm}$ boule is presented in Figure 5 and chosen as the sample to assess the crystal structural quality. Five locations/regions of the wafer were chosen for characterization, as shown in Figure 5b. The root mean square roughness of the wafer surface was identified to be 0.185 nm for a $5 \mu\text{m} \times 5 \mu\text{m}$ area via atomic force microscopy (Veeco Dimension 3100 V), and no scratches, pits, or other polishing-induced defects were observed (as shown in Figure 6).

HRXRD rocking curves (omega scan) were obtained by using an X-ray diffractometer (Bruker D8 Discover) using symmetric ((0002)) and asymmetrical ($(10\bar{1}2)$) reflections. Raman spectroscopy was employed to estimate the structural quality of the crystals and the residual stress inside the crystals. Optical absorption spectra were acquired with a UV/visible spectrometer (PerkinElmer Lambda 19) at room temperature.

In general, threading screw and edge dislocations (corresponding to tilting and twisting of the lattice, respectively) in crystals can result in the broadening of the (0002) and $(10\bar{1}2)$

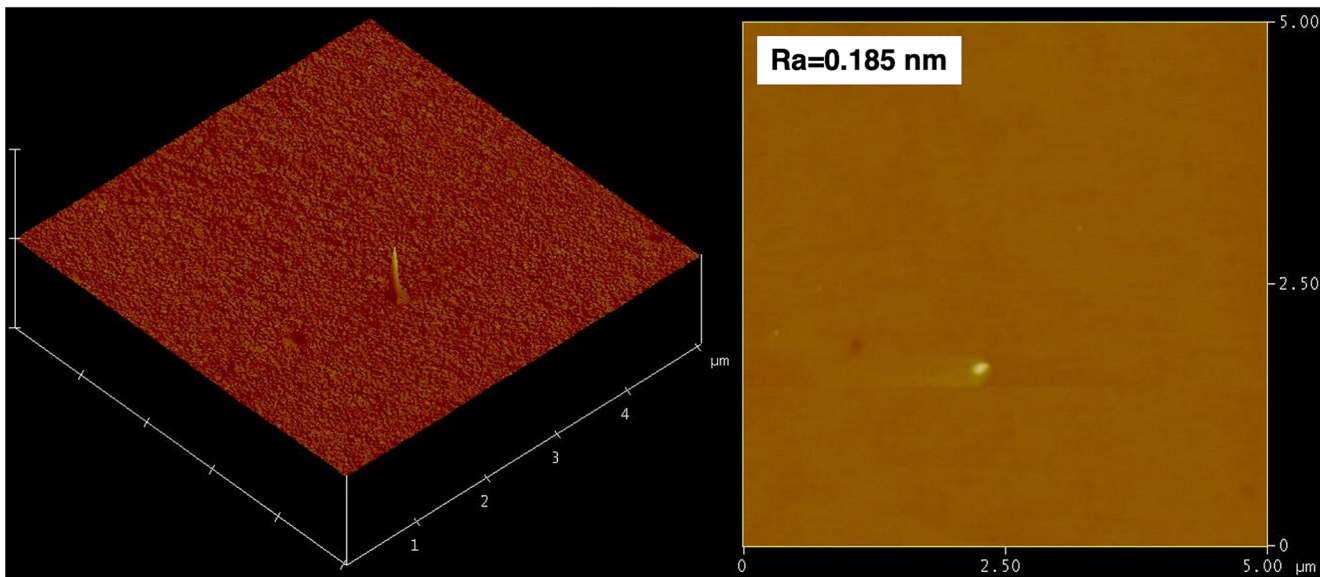


Figure 6. AFM scan of a microscale region of a 2 in. AlN sample wafer after CMP.

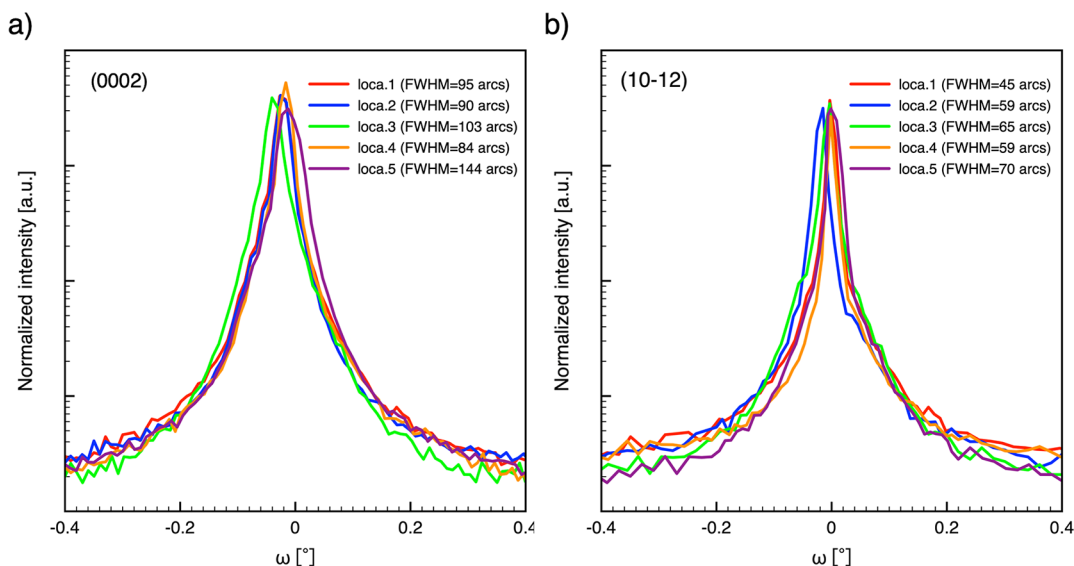


Figure 7. X-ray rocking curves of a 2 in. AlN sample wafer: (a) symmetric (0002) reflection and (b) asymmetric (10 $\bar{1}$ 2) reflection.

rocking curves. Accordingly, the crystal quality was further assessed by HRXRD ω -oscillation curves of (0002) symmetric and (10 $\bar{1}$ 2) asymmetric reflections. As illustrated in Figure 7, the fwhms of the (0002) and (10 $\bar{1}$ 2) rocking curves are 84–144 arcsec and 45–70 arcsec, respectively. These data show a significant improvement in the uniformity of the crystal quality compared to our previous report,¹⁸ although these results are still marginally inferior to those reported in the literature for 2 in. wafers.¹⁶

Figure 8 shows the Raman spectra of the 2 in. wafer at five positions, where the phonon modes follow the C_{6v} point group symmetry rule corresponding to the scattering configuration. Three high-intensity phonon modes, E2(low), E2(high), and A1(LO), are observed, and the spectra obtained at the five positions are almost identical. In particular, the fwhm and peak position of E2(high) are usually used to indicate the structure quality of crystals and the stress in crystals, respectively. In this work, the Raman frequency of the E2(high) mode is 657 cm^{-1} , which is close to the unstressed AlN Raman frequency (657 cm^{-1} ,

cm^{-1}),^{42,43} indicating the presence of low tensile stress in the crystal. The fwhm of the E2(high) mode is determined to be 5.4–5.8 cm^{-1} .

To further study the structural defects in the AlN crystal, AlN wafers were selectively wet etched at 360 °C for 5 min in a eutectic KOH/NaOH solution. Scanning electron microscopy (SEM) was used to characterize the surface morphology of the 2 in. Al-polar AlN sample wafer after selective wet etching (Figure 9). The etch pit density (EPD) varies from 10^4 to 10^6 cm^{-2} , and the typical average EPD is approximately 8.5×10^4 cm^{-2} .

With a band gap up to 6.2 eV, AlN exhibits unique advantages in the DUV band. AlN-based UV-LED devices can be used in the full UV band from 200 to 400 nm. In the disinfection process of UVC-LEDs, the germicidal effect of UV radiation is most evident in the wavelength range of 260–280 nm.^{2,3,18} The low DUV transmittance of AlN substrates has been regarded as a barrier to their application due to their extraction of light in current UV-LED layouts.¹⁷ Bickermann et

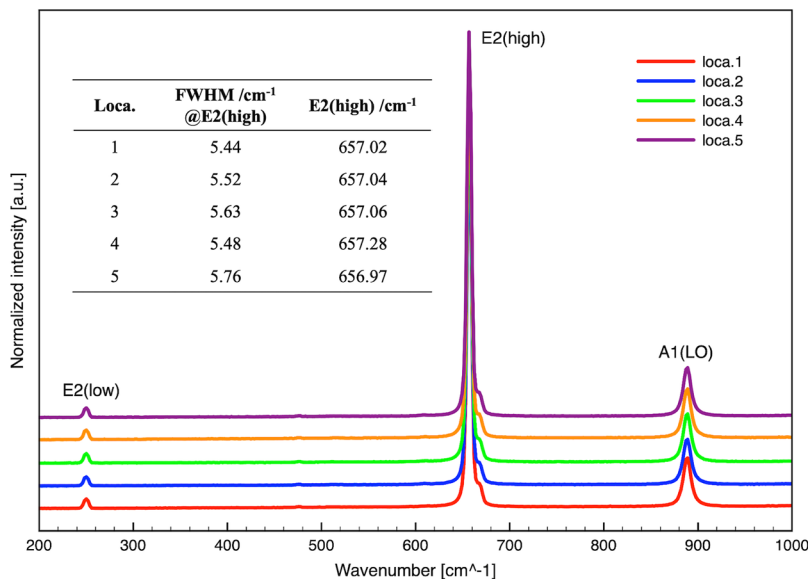


Figure 8. Raman spectra along the radial direction of a 2 in. *c*-plane AlN sample wafer.

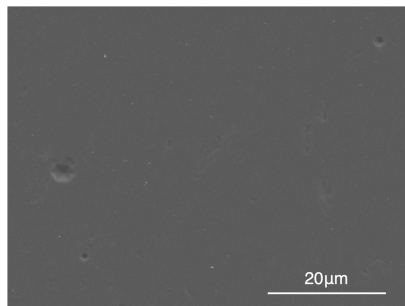


Figure 9. SEM micrograph of a 2 in. Al-polar AlN sample wafer after etching in eutectic KOH/NaOH (average EPD $\approx 8.5 \times 10^4 \text{ cm}^{-2}$).

al.^{44,45} reported an absorption coefficient (AC) of 12–18 cm^{−1} at wavelengths between 220 and 380 nm, representing approximately 80% of the total area of 22 mm-diameter AlN wafers. Very recently, Bondokov et al.⁴⁶ reported 2 in. AlN wafers with ACs below 10.5 cm^{−1} at a 265 nm wavelength. Figure 10 illustrates that the ACs in the range of 200–1000 nm measured by UV-vis–NIR spectroscopy for the 2 in. sample wafer are 19–29 cm^{−1} in the DUV range (260–280 nm), demonstrating high uniformity.

To track the structural quality evolution during homoepitaxial growth of the Al-polar AlN crystals, the AlN boule shown in Figure 4 was sliced into *c*-plane wafers with a typical thickness of 600 μm . The distribution of symmetric reflection fwhms for different crystal axial positions in the wafer is shown in Figure

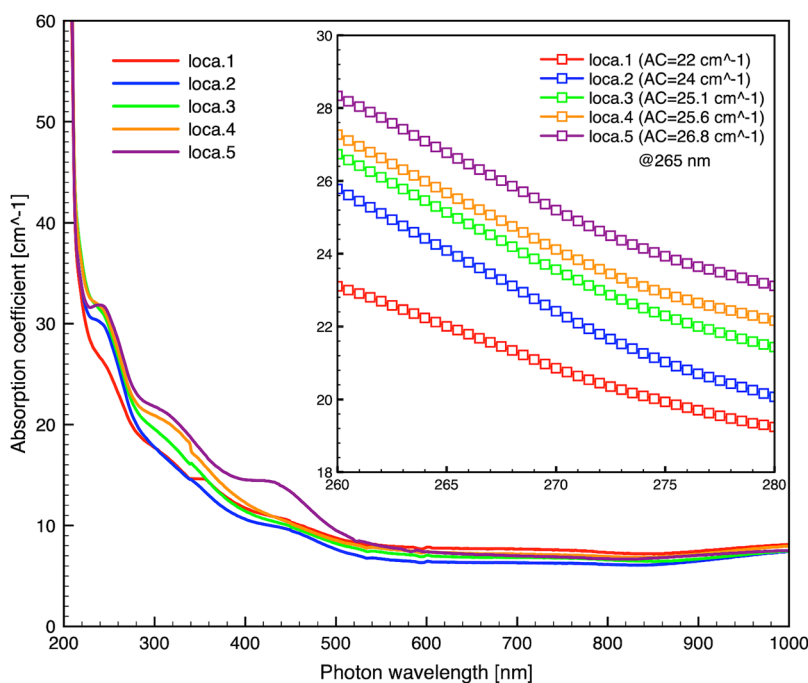


Figure 10. Absorption spectra of five different locations of a 2 in. sample wafer.

11. The crystal quality of the central region is higher than that of the edge region, which can be attributed to additional

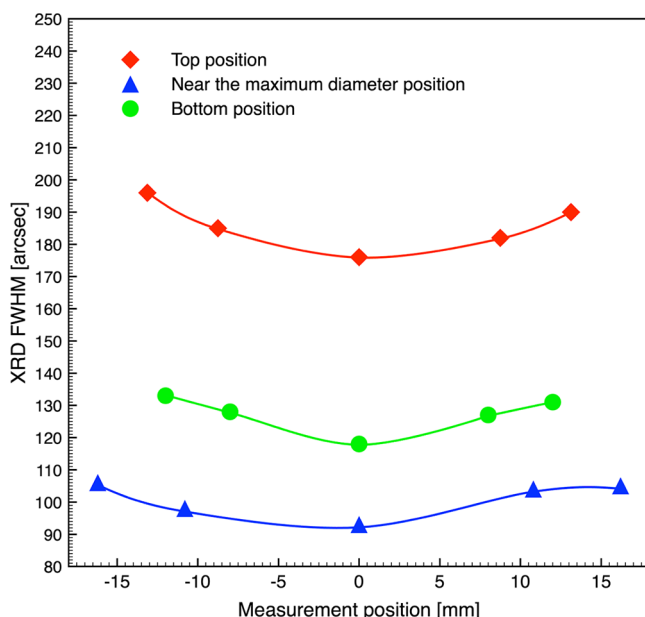


Figure 11. Evolution of the symmetric reflection fwhms of a 47 mm AlN boule.

defects such as LAGBs or BPDs nucleated at the boule edge (or diameter expansion regions). For the wafers grown at the rapid diameter expansion stage, a relatively lower structural quality ($\text{fwhm} \sim 130 \text{ arcsec}$) was identified. With the formation of m -planes, the quality improved steadily, and the symmetric reflection fwhms at all positions were less than 110 arcsec. Nevertheless, there was substantial structural quality deterioration after the formation of r -planes.

5. CONCLUSIONS

Crack-free Al-polar AlN single crystals up to $\Phi 56 \text{ mm}$ were prepared using a homoepitaxial growth technique by the PVT method for the first time. The crystal growth habit and the diameter enlargement behavior of Al-polar boules were investigated. Our growth experiments showed that stable step-flow growth of large Al-polar crystals with good structural quality and UV transparency was possible using a pure tungsten setup. The initial expansion angle reached $50\text{--}60^\circ$ and then gradually decreased to $10\text{--}20^\circ$ under reasonable growth conditions during the growth process. The radial temperature gradient plays a dominant role in the crystal growth habit. Large radial temperature gradients can suppress the formation of $\{10\bar{1}0\}$ facets. The central region of the crystals always maintained very similar quality as the seeds, while slight growth deterioration at the crystal periphery was observed. Raman spectra showed an E2(high) fwhm of $5.44\text{--}5.76 \text{ cm}^{-1}$. The symmetric and asymmetric HRXRD rocking curves showed fwhms of $84\text{--}144$ and $45\text{--}70 \text{ arcsec}$, respectively. The average EPD evaluated by preferential chemical etching was approximately $8.5 \times 10^4 \text{ cm}^{-2}$. The optical transmission spectra revealed that the entire wafer exhibits excellent UV transparency, with absorption coefficients of $19\text{--}29 \text{ cm}^{-1}$ in the UV range of $4.43\text{--}4.77 \text{ eV}$ ($260\text{--}280 \text{ nm}$).

AUTHOR INFORMATION

Corresponding Authors

Jiang Wang – State Key Laboratory of Advanced Special Steel & Shanghai Key Laboratory of Advanced Ferrometallurgy & School of Materials Science and Engineering, Shanghai University, Shanghai 200072, China; Phone: 021-66138061; Email: jiangwang@i.shu.edu.cn

Liang Wu – Ultratrend Technologies Inc., Hangzhou City, Zhejiang Province 311199, China; Phone: 0086-18516773360; Email: Jason.wu@utrendtech.com

Authors

Danyang Fu – Ultratrend Technologies Inc., Hangzhou City, Zhejiang Province 311199, China; State Key Laboratory of Advanced Special Steel & Shanghai Key Laboratory of Advanced Ferrometallurgy & School of Materials Science and Engineering, Shanghai University, Shanghai 200072, China; orcid.org/0000-0001-8574-4970

Dan Lei – Ultratrend Technologies Inc., Hangzhou City, Zhejiang Province 311199, China

Zhe Li – State Key Laboratory of Advanced Special Steel & Shanghai Key Laboratory of Advanced Ferrometallurgy & School of Materials Science and Engineering, Shanghai University, Shanghai 200072, China

Gang Zhang – State Key Laboratory of Advanced Special Steel & Shanghai Key Laboratory of Advanced Ferrometallurgy & School of Materials Science and Engineering, Shanghai University, Shanghai 200072, China

Jiali Huang – Ultratrend Technologies Inc., Hangzhou City, Zhejiang Province 311199, China

Xiaojuan Sun – State Key Laboratory of Luminescence and Applications, Changchun Institute of Optics, Fine Mechanics and Physics, Chinese Academy of Sciences, Changchun 130033, China; Center of Materials Science and Optoelectronics Engineering, University of Chinese Academy of Sciences, Beijing 100049, China

Qikun Wang – Ultratrend Technologies Inc., Hangzhou City, Zhejiang Province 311199, China

Dabing Li – State Key Laboratory of Luminescence and Applications, Changchun Institute of Optics, Fine Mechanics and Physics, Chinese Academy of Sciences, Changchun 130033, China; Center of Materials Science and Optoelectronics Engineering, University of Chinese Academy of Sciences, Beijing 100049, China; orcid.org/0000-0001-5353-1460

Complete contact information is available at:
<https://pubs.acs.org/10.1021/acs.cgd.2c00240>

Funding

The authors cordially acknowledge financial support from the National Natural Science Foundation of China (Grant nos. 61874071, 61725403, 61827813, and 62121005) and the Key Research and Development Program of Zhejiang Province (2020C01145).

Notes

The authors declare no competing financial interest.

REFERENCES

- (1) Ambacher, O. Growth and applications of Group III-nitrides. *J. Phys. D: Appl. Phys.* **1998**, *31*, 2653–2710.
- (2) Yu, R.; Liu, G.; Wang, G.; Chen, C.; Xu, M.; Zhou, H.; Wang, T.; Yu, J.; Zhao, G.; Zhang, L. Ultrawide-bandgap semiconductor AlN

- crystals: growth and applications. *J. Mater. Chem. C* **2021**, *9*, 1852–1873.
- (3) Tsao, J. Y.; Chowdhury, S.; Hollis, M. A.; Jena, D.; Johnson, N. M.; Jones, K. A.; Kaplar, R. J.; Rajan, S.; Van de Walle, C. G.; Bellotti, E.; Chua, C. L.; Collazo, R.; Coltrin, M. E.; Cooper, J. A.; Evans, K. R.; Graham, S.; Grotjohn, T. A.; Heller, E. R.; Higashiwaki, M.; Islam, M. S.; Juodawlkis, P. W.; Khan, M. A.; Koehler, A. D.; Leach, J. H.; Mishra, U. K.; Nemanich, R. J.; Pilawa-Podgurski, R. C. N.; Shealy, J. B.; Sitar, Z.; Tadjer, M. J.; Witulski, A. F.; Wraback, M.; Simmons, J. A. Ultrawide-Bandgap Semiconductors: Research Opportunities and Challenges. *Adv. Electron. Mater.* **2018**, *4*, 1600501.
- (4) Fu, D.; Gong, J.; Lei, D.; Huang, J.; Wang, Q.; Wu, L. Recent Progress and Future Challenges of AlN Single Crystal Growth by Physical Vapor Transport. *J. Synth. Cryst.* **2020**, *49*, 1141–1156.
- (5) Katagiri, Y.; Kishino, S.; Okura, K.; Miyake, H.; Hiramatu, K. Low-pressure HVPE growth of crack-free thick AlN on a trench-patterned AlN template. *J. Cryst. Growth* **2009**, *311*, 2831–2833.
- (6) Kumagai, Y.; Tajima, J.; Ishizuki, M.; Nagashima, T.; Murakami, H.; Takada, K.; Koukitu, A. Self-Separation of a Thick AlN Layer from a Sapphire Substrate via Interfacial Voids Formed by the Decomposition of Sapphire. *Appl. Phys. Express* **2008**, *1*, 045003.
- (7) Freitas, J. A. Properties of the state of the art of bulk III-V nitride substrates and homoepitaxial layers. *J. Phys. D: Appl. Phys.* **2010**, *43*, 073001.
- (8) Kamei, K.; Shirai, Y.; Tanaka, T.; Okada, N.; Yauchi, A.; Amano, H. Solution growth of AlN single crystal using Cu solvent under atmospheric pressure nitrogen. *Phys. Status Solidi C* **2007**, *4*, 2211–2214.
- (9) Bockowski, M. Growth and doping of GaN and AlN single crystals under high nitrogen pressure. *Cryst. Res. Technol.* **2001**, *36*, 771–787.
- (10) Kangawa, Y.; Toki, R.; Yayama, T.; Epelbaum, B. M.; Kakimoto, K. Novel solution growth method of bulk AlN using Al and Li₃N solid sources. *Appl. Phys. Express* **2011**, *4*, 095501.
- (11) Slack, G. A.; McNelly, T. F. Growth of high purity AlN crystals. *J. Cryst. Growth* **1976**, *34*, 263–279.
- (12) Hartmann, C.; Dittmar, A.; Wollweber, J.; Bickermann, M. Bulk AlN growth by physical vapour transport. *Semicond. Sci. Technol.* **2014**, *29*, 084002.
- (13) Bondokov, R. T.; Mueller, S. G.; Morgan, K. E.; Slack, G. A.; Schujman, S.; Wood, M. C.; Smart, J. A.; Schowalter, L. J. Large-area AlN substrates for electronic applications: An industrial perspective. *J. Cryst. Growth* **2008**, *310*, 4020–4026.
- (14) Mueller, S. G.; Bondokov, R. T.; Morgan, K. E.; Slack, G. A.; Schujman, S. B.; Grandusky, J.; Smart, J. A.; Schowalter, L. J. The progress of AlN bulk growth and epitaxy for electronic applications. *Phys. Status Solidi A* **2009**, *206*, 1153–1159.
- (15) Schujman, S. B.; Schowalter, L. J.; Bondokov, R. T.; Morgan, K. E.; Liu, W.; Smart, J. A.; Bottles, T. Structural and surface characterization of large diameter, crystalline AlN substrates for device fabrication. *J. Cryst. Growth* **2008**, *310*, 887–890.
- (16) Dalmau, R.; Craft, H. S.; Britt, J.; Paisley, E.; Moody, B.; Guo, J. Q.; Ji, Y. J.; Raghorthamachar, B.; Dudley, M.; Schlessner, R. High quality AlN single crystal substrates for AlGaN-based devices. *Mater. Sci. Forum* **2018**, *924*, 923–926.
- (17) Wang, Q.; Lei, D.; He, G.; Gong, J.; Huang, J.; Wu, J. Characterization of 60 mm AlN Single Crystal Wafers Grown by the Physical Vapor Transport Method. *Phys. Status Solidi A* **2019**, *216*, 1900118.
- (18) Hartmann, C.; Wollweber, J.; Sintonen, S.; Dittmar, A.; Kirste, L.; Kollowa, S.; Irmscher, K.; Bickermann, M. Preparation of deep UV transparent AlN substrates with high structural perfection for optoelectronic devices. *CrystEngComm* **2016**, *18*, 3488–3497.
- (19) Filip, O.; Epelbaum, B. M.; Bickermann, M.; Heimann, P.; Winnacker, A. Effects of growth direction and polarity on bulk aluminum nitride crystal properties. *J. Cryst. Growth* **2011**, *318*, 427–431.
- (20) Bickermann, M.; Epelbaum, B. M.; Filip, O.; Heimann, P.; Nagata, S.; Winnacker, A. Point defect content and optical transitions in bulk aluminum nitride crystals. *Phys. Status Solidi B* **2009**, *246*, 1181–1183.
- (21) Nyakiti, L. O.; Lee, R. G.; Gu, Z.; Edgar, J. H.; Chaudhuri, J. Polarity determination of rough and smooth surface grains in AlN crystals. *Cryst. Res. Technol.* **2012**, *47*, 1134–1139.
- (22) Hartmann, C.; Wollweber, J.; Dittmar, A.; Irmscher, K.; Kwasniewski, A.; Langhans, F.; Neugut, T.; Bickermann, M. Preparation of Bulk AlN Seeds by Spontaneous Nucleation of Freestanding Crystals. *Jpn. J. Appl. Phys.* **2013**, *52*, 08JA06.
- (23) Herro, Z. G.; Zhuang, D.; Schlessner, R.; Sitar, Z.; Sitar, Z. Growth of AlN single crystalline boules. *J. Cryst. Growth* **2010**, *312*, 2519–2521.
- (24) Herro, Z. G.; Zhuang, D.; Schlessner, R.; Collazo, R.; Sitar, Z. Seeded growth of AlN on N- and Al-polar <0001> AlN seeds by physical vapor transport. *J. Cryst. Growth* **2006**, *286*, 205–208.
- (25) Bickermann, M.; Epelbaum, B. M.; Filip, O.; Tautz, B.; Heimann, P.; Winnacker, A. Faceting in AlN bulk crystal growth and its impact on optical properties of the crystals. *Phys. Status Solidi C* **2012**, *9*, 449–452.
- (26) Wang, Z. H.; Deng, X. L.; Cao, K.; Wang, J.; Wu, L. Hotzone design and optimization for 2-in. AlN PVT growth process through global heat transfer modeling and simulations. *J. Cryst. Growth* **2017**, *474*, 76–80.
- (27) Fu, D.; Wang, Q.; Zhang, G.; Zhu, R.; Liu, H.; Li, Z.; Wu, L. Modelling and simulation of oxygen transport during AlN crystal growth by the PVT method. *J. Cryst. Growth* **2020**, *551*, 125902.
- (28) Wang, Q.; Huang, J.; Fu, D.; He, G.; Lei, D.; Wu, L. Influence of crucible shape on mass transport in AlN crystal growth by physical vapor transport process. *J. Cryst. Growth* **2019**, *515*, 21–25.
- (29) Raghorthamachar, B.; Yang, Y.; Dalmau, R.; Moody, B.; Craft, H. S.; Schlessner, R.; Dudley, M.; Sitar, Z. Defect generation mechanisms in PVT-grown AlN single crystal boules. *Mater. Sci. Forum* **2013**, *740*–742, 91–94.
- (30) Dalmau, R.; Moody, B.; Xie, J.; Collazo, R.; Sitar, Z. Characterization of dislocation arrays in AlN single crystals grown by PVT. *Phys. Status Solidi A* **2011**, *208*, 1545–1547.
- (31) Langhans, F.; Kiefer, S.; Hartmann, C.; Markurt, T.; Schulz, T.; Gugushev, C.; Naumann, M.; Kollowa, S.; Dittmar, A.; Wollweber, J.; Bickermann, M. Precipitates originating from tungsten crucible parts in AlN bulk crystals grown by the PVT method. *Cryst. Res. Technol.* **2016**, *51*, 129–136.
- (32) Fu, D.; Wang, Q.; Zhang, G.; Li, Z.; Huang, J.; Wang, J.; Wu, L. Influences of Powder Source Porosity on Mass Transport during AlN Crystal Growth Using Physical Vapor Transport Method. *Crystals* **2021**, *11*, 1436.
- (33) Wang, Q.; Huang, J.; Wang, Z.; He, G.; Lei, D.; Gong, J.; Wu, L. Anisotropic Three-Dimensional Thermal Stress Modeling and Simulation of Homoepitaxial AlN Single Crystal Growth by the Physical Vapor Transport Method. *Cryst. Growth Des.* **2018**, *18*, 2998–3007.
- (34) Wang, Q.; Zhao, Y.; Huang, J.; Fu, D.; He, G.; Wu, L. Optimization of total resolved shear stress in AlN single crystals homoepitaxially grown by physical vapor transport method. *J. Cryst. Growth* **2019**, *519*, 14–19.
- (35) Zhao, Y.; Wang, Q.; Zhang, G.; Huang, J.; Fu, D.; Wu, J. Comparison of the Thermal Stress Behavior of AlN Single Crystal Growth on AlN and SiC Seeds via the Physical Vapor Transport Method through Three-Dimensional Numerical Modeling and Simulation. *Cryst. Growth Des.* **2021**, *21*, 2653–2662.
- (36) Zhang, G.; Fu, D.; Li, Z.; Huang, J.; Wang, Q.; Ren, Z.; Wu, L. Effects of seed-holder shape on the initial growth of AlN crystals by homoepitaxial PVT method. *J. Synth. Cryst.* **2022**, *51*, 27–34.
- (37) Wang, Z.; Wang, Q.; He, G.; Lei, D.; Huang, J.; Wu, L. Characterization of freestanding AlN single crystals grown through a novel approach using the PVT method. *Rare Met. Mater. Eng.* **2019**, *48*, 403–408.
- (38) Lu, P.; Collazo, R.; Dalmau, R. F.; Durkaya, G.; Dietz, N.; Raghorthamachar, B.; Dudley, M.; Sitar, Z. Seeded growth of AlN bulk crystals in m- and c-orientation. *J. Cryst. Growth* **2009**, *312*, 58–63.

- (39) Makarov, Y. N.; Avdeev, O. V.; Barash, I. S.; Bazarevskiy, D. S.; Chemekova, T. Y.; Mokhov, E. N.; Nagalyuk, S. S.; Roenkov, A. D.; Segal, A. S.; Vodakov, Y. A.; Ramm, M. G.; Davis, S.; Huminic, G.; Helava, H. Experimental and theoretical analysis of sublimation growth of AlN bulk crystals. *J. Cryst. Growth* **2008**, *310*, 881–886.
- (40) Hartmann, C.; Wollweber, J.; Seitz, C.; Albrecht, M.; Fornari, R. Homoepitaxial seeding and growth of bulk AlN by sublimation. *J. Cryst. Growth* **2008**, *310*, 930–934.
- (41) Chemekova, T. Y.; Avdeev, O. V.; Barash, I. S.; Mokhov, E. N.; Nagalyuk, S. S.; Roenkov, A. D.; Segal, A. S.; Makarov, Y. N.; Ramm, M. G.; Davis, S.; Huminic, G.; Helava, H. Sublimation growth of 2 inch diameter bulk AlN crystals. *Phys. Status Solidi C* **2008**, *5*, 1612–1614.
- (42) Kuball, M.; Hayes, J. M.; Shi, Y.; Edgar, J. H.; Prins, A. D.; van Uden, N. W. A.; Dunstan, D. J. Raman scattering studies on single-crystalline bulk AlN: temperature and pressure dependence of the AlN phonon modes. *J. Cryst. Growth* **2001**, *231*, 391–396.
- (43) Davydov, V. Y.; Kitaev, Y. E.; Goncharuk, I. N.; Smirnov, A. N.; Graul, J.; Semchinova, O.; Uffmann, D.; Smirnov, M. B.; Mirgorodsky, A. P.; Evgrestov, R. A. Phonon dispersion and Raman scattering in hexagonal GaN and AlN. *Phys. Rev. B: Condens. Matter Mater. Phys.* **1998**, *58*, 12899–12909.
- (44) Bickermann, M.; Epelbaum, B. M.; Filip, O.; Heimann, P.; Feneberg, M.; Nagata, S.; Winnacker, A. Deep-UV transparent bulk single-crystalline AlN substrates. *Phys. Status Solidi C* **2010**, *7*, 1743–1745.
- (45) Bickermann, M.; Epelbaum, B. M.; Filip, O.; Heimann, P.; Nagata, S.; Winnacker, A.; Winnacker, A. UV transparent single-crystalline bulk AlN substrates. *Phys. Status Solidi C* **2010**, *7*, 21–24.
- (46) Bondokov, R. T.; Branagan, S. P.; Ishigami, N.; Grandusky, J.; Nagatomi, T.; Tatsuta, K.; Miebach, T.; Chen, J. Two-Inch Aluminum Nitride (AlN) Single Crystal Growth for Commercial Applications. *ECS Trans.* **2021**, *104*, 37–48.

□ Recommended by ACS

Chlorine-Assisted Growth of Epitaxial InGaN and AlGaN Crystals at Low Temperatures Using Plasma-Enhanced Chemical Vapor Deposition

Chun-Wei Chuang and Franklin Chau-Nan Hong

DECEMBER 21, 2022

CRYSTAL GROWTH & DESIGN

READ ▶

AlGaN UV Detector with Largely Enhanced Heat Dissipation on Mo Substrate Enabled by van der Waals Epitaxy

Yang Chen, Dabing Li, *et al.*

DECEMBER 23, 2022

CRYSTAL GROWTH & DESIGN

READ ▶

Pulsed-Mode MOCVD Growth of ZnSn(Ga)N₂ and Determination of the Valence Band Offset with GaN

Kaitian Zhang, Hongping Zhao, *et al.*

JULY 08, 2022

CRYSTAL GROWTH & DESIGN

READ ▶

Growth of Large Ti:Sapphire Crystals by the Method of HDC with Gradient Doping

Sergii Nizhankovskyi, Igor Pritula, *et al.*

OCTOBER 27, 2022

CRYSTAL GROWTH & DESIGN

READ ▶

[Get More Suggestions >](#)